ELSEVIER

Journal of Wind Engineering
and Industrial Aerodynamics 89 (2001) 1383–1395

JOURNAL OF wind engineering AND industrial aerodynamics

www.elsevier.com/locate/jweia

Influence of free-stream turbulence on the movement-induced vibrations of an elongated rectangular cylinder in cross-flow

P. Hémon[a,*], F. Santi[a], B. Schnoerringer[b], J. Wojciechowski[c]

[a] *Institut AéroTechnique/CNAM, 15 rue Marat, 78210 Saint-Cyr L'Ecole, France*
[b] *ESSTIN Nancy, Parc Robert Bentz, rue jean hamour, 54500 Vandoeuvre, France*
[c] *Warsaw University of Technology, Dept. of Aerodynamics, ul. Nowowiejska 24, 00-665 Warsaw, Poland*

Abstract

We present an experimental study of the galloping oscillations of an elongated cylinder. The shape ratio of the rectangular section is 1:2 and we study the influence of free-stream turbulence on the vibrations. The main studied parameter is the turbulence intensity. In smooth flow, the structure is also submitted to vortex shedding lock-in, which disappears in turbulent flow. At low intensity (4–5%), the critical velocity decreases by comparison with smooth flow. A jump of the Strouhal number is reported and can explain this decrease. At 6% intensity, the critical velocity increases, then the system becomes stable at 7.5%.

Keywords: Galloping; Rectangular cylinder; Turbulence; Aeroelasticity

1. Introduction

We consider the galloping oscillations of an elongated cylinder submitted to a cross-flow. The section is rectangular with a shape ratio $c/e = 2$ as shown in Fig. 1. This section is a critical configuration because the reattachment on the lateral sides depends on the free-stream turbulence.

Indeed, the fact that the reattachment occurs (or not) has the effect of producing a positive (or negative) lift slope, which will stabilise (or excite) the galloping oscillations [1]. The influence of turbulence is therefore interesting to study, and some previous works have been published: some of them are devoted to larger shape

*Corresponding author. Tel.: +33-1-30-458619; fax: +33-1-30-458610.
E-mail address: hemon@iat.cnam.fr (P. Hémon).

0167-6105/01/$ - see front matter
PII: S0167-6105(01)00126-X

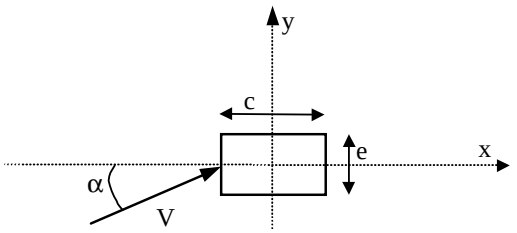

Fig. 1. Configuration of the study.

ratio [2] or to smaller ones [3–5]. One has also to mention the pioneering work of Ref. [6] who first reported the effect of turbulence on the galloping of rectangular cylinders.

On large shape ratio, it was shown in Ref. [7] that the reattachment is earlier when the intensity of turbulence is increased. Our choice of the section $c/e = 2$ is justified because the turbulence intensity should be an important parameter with regard to galloping.

Anyway, the experimental studies of vibrations are often more devoted to the vortex shedding lock-in [8,9] and the galloping regime is less investigated.

Otherwise, the work presented in Ref. [10] was devoted to the study of general variation of the angle of attack α, with 2D and 3D (clamped-free) models, between 0 and 90°. However, the behaviour is very different for the small values of the angle α and we will investigate this region more accurately.

The objective of the paper is then to present the experimental study of the galloping oscillations and the influence of the free-stream turbulence. An important point, which makes this work different from other authors, is the use of free vibrations of an elongated flexible cylinder. More generally, this work has the objective of increasing the physical understanding of this kind of flow-structure interaction in order to develop and validate mechanical modelling for prediction, such as in Ref. [11].

2. Experimental setup

2.1. Wind tunnel

The test were carried out in a small wind tunnel of the Institut Aérotechnique. The test square section has a width (D) of 0.6 m and a length of 2 m. Velocity can vary from 4 to 30 m/s. A single channel hot wire anemometer was mounted for turbulence and wake investigations. Its non linear calibration curve is a 4 order polynomial. Data acquisition was performed on a PC using a high-speed A/D converter with a sampling frequency up to 400 kHz.

The turbulence intensity (I) in the standard configuration is between 0.4% and 0.5% as shown in Fig. 2. The corresponding longitudinal correlation length (Lx) was

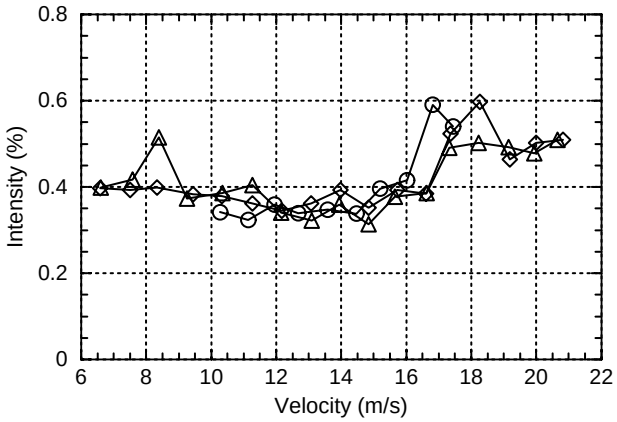

Fig. 2. Turbulence intensity versus wind velocity for the smooth flow configuration.

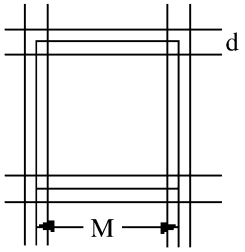

Fig. 3. Parameters of the square grid.

calculated using the Taylor hypothesis on the basis of measurements of the integral time scale.

For the range of velocities [4–17 m/s] of the present study, Lx is greater than the thickness of the rectangular cylinder and Lx/e is found in the range [5–8]. The corresponding time scale of the turbulence is smaller than the vibration period of the cylinder, with a ratio between 0.1 and 0.05.

In order to generate turbulence, a square grid was mounted in the beginning of the test section (see Fig. 3). This grid was inspired from Refs. [3,12]. The mesh size M is equal to 60 mm and is built with a square rod of 9 mm. The size of the test section is then 10 M, and the longitudinal positions x/M investigated were 10, 13 16 19 and 22. The resulting turbulence intensities were respectively, 7.5%, 6, 5%, 4.5% and 4% as is presented in Fig. 4. The empirical relation that is also plotted is of the form

$$I^2 = \frac{1}{30}\left(\frac{x}{M} - 4\right)^{-1.1}.$$

The time macro-scale was measured using two methods: (i) with the autocorrelation function given after a long duration of averaging by a spectrum analyser and, (ii) the power spectrum at zero frequency. The results were consistent in both cases. The

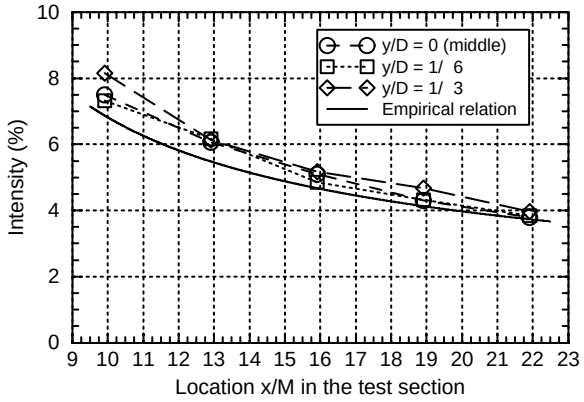

Fig. 4. Turbulence intensity versus locations x/M in the test section for different lateral positions y/D.

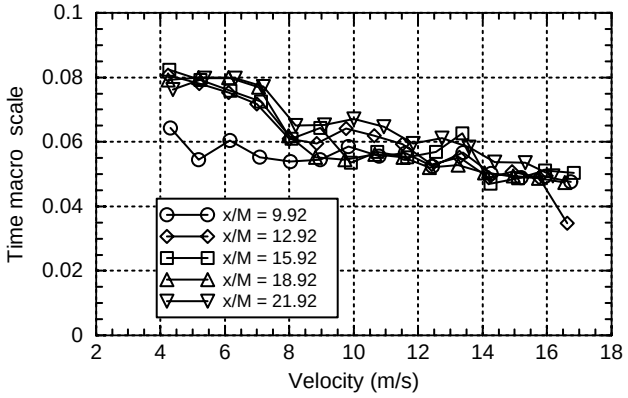

Fig. 5. Reduced time macro-scale versus wind velocity at different locations x/M in the test section.

time scale reduced by the first period of vibration of the model (1/27 s) is given in Fig. 5. One may note that this time scale is smaller than the period of vibration. By using the Taylor hypothesis of isotropic and homogeneous turbulence, the longitudinal macro-scale Lx is deduced and plotted in Fig. 6. It is reduced by the thickness e of the beam model.

It should be noticed that the regime seems unchanged with and without the grid because Lx/e was found in the range [2–6] in the turbulent case. Then the size of the turbulent eddies is just only greater than the size of the cylinder. The study will focus on the effects of the turbulence intensity.

2.2. Vibrating model

The model tested is a rectangular beam clamped at both extremities (Fig. 7). The dimensions are $c = 10\,\text{mm}$, $e = 5\,\text{mm}$ and its length is 950 mm. It is made of

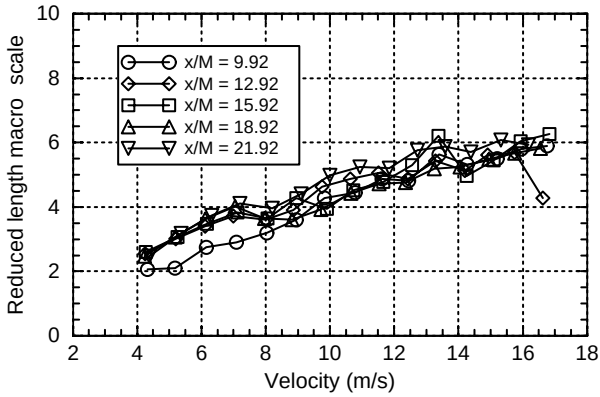

Fig. 6. Reduced length macro-scale Lx/e versus wind velocity at different locations x/M in the test section.

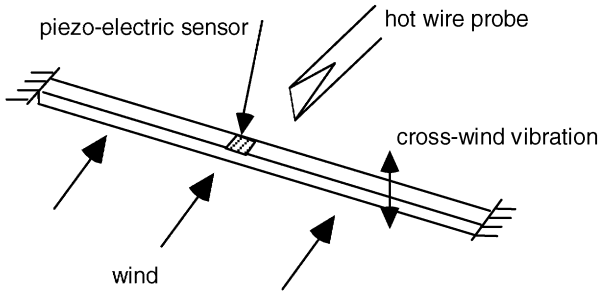

Fig. 7. Principle of the wind tunnel tests.

aluminium alloy and its first bending frequency is $f = 27$ Hz. The clamping system was specially designed in order to reach *ideal clamping* and to allow a variation of the angle of incidence ($\pm 30^\circ$). The results of computations of the eigenfrequencies by a finite element code were found to be in very good agreement with the measurements, with a difference less than 1%.

The free vibrations were measured using piezo-electric sensors glued on the beam. It is a 40 μm thick PVDF film glued to the middle upper face of the beam. It is connected to the acquisition system through a charge amplifier and an analog filter. The charge amplifier is wired so as to deliver a dynamic signal representing the velocity of the structure at the location of the sensor, thus the signal voltage is zero when the beam is not moving. This measuring method was chosen in order to eliminate zero shift problems due to thermal or pre-stress effects which are critical points when applying piezo-electric techniques.

However, the calibration of such a system becomes more complex since it needs to be done dynamically. A mass was suspended to the beam and then allowed to fall. The free damped vibrations were recorded with the piezo-electric sensor. The reference solution was given by a finite element computation using a Timoshenko

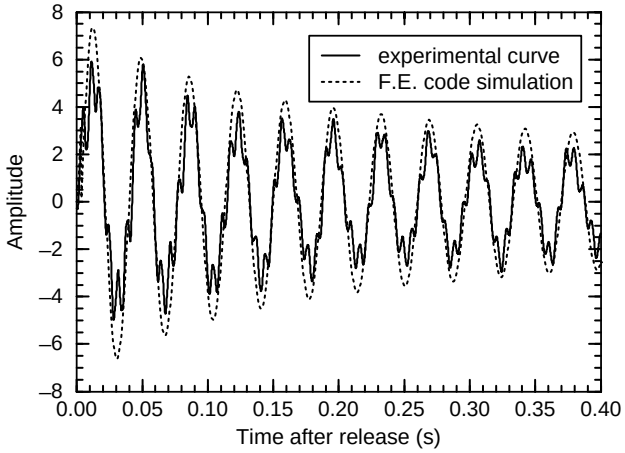

Fig. 8. Dynamic calibration results.

beam model. Fig. 8 gives an example of calibration results after introducing the structural damping and the calibration coefficient of the piezo-electric sensor.

It should be noted that the system measures the response of more than one eigenmode whereas the numerical solution is based on the first mode only. This is due to the fact that the sensor has a size in its spanwise direction which is not negligible: it is not the case of the reference signal given for a node of the discretization by finite elements.

Measurements of the structural damping (0.24% of the critical damping) lead to a Scruton number equal to 22. In the whole paper, the reference length is the thickness e of the beam (5 mm). The corresponding Reynolds number of the tests is in the range [1500–5000].

In the following, the vibrations results will be given for the middle of the beam and represent the dimensionless oscillation velocity in y direction (see Fig. 1) versus the reduced wind velocity. The reference frequency is the first bending frequency f of the cylinder (27 Hz). The amplitude of the velocity is the root mean square value (RMS) which in practice represents around 71% of the maximum value.

3. Results of experiments

3.1. Strouhal numbers

The Strouhal number of the alternate vortex shedding was measured behind the beam without vibration with a hot wire probe connected to a spectrum analyser. The result is plotted in Fig. 9 versus the angle of attack and with the turbulence intensity as the parameter.

At 0° and smooth flow, the result is in agreement with those reported in Refs. [8,13] and is due to impinging leading-edge vortices. The jump at the

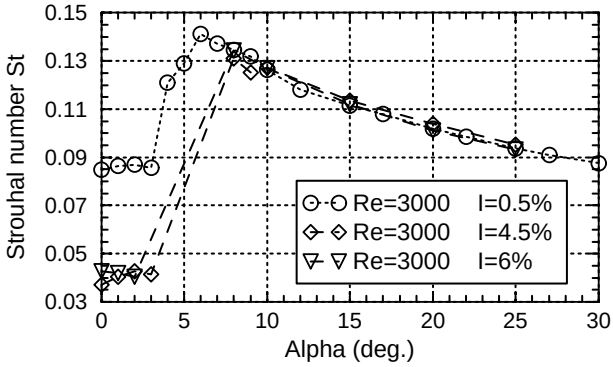

Fig. 9. Measured Strouhal number.

angle 4–6° is linked to a change in a pure shedding of leading-edge vortices for higher angles.

In turbulent cases, the peak in the power spectrum of the velocity was less dominant and a long time of averaging was necessary for the small angles of attack. The impingement of the leading-edge vortices becomes less periodic with increasing turbulence. Between 4 and 8°, no significant peak can be detected which means that no coherent and periodic impinging leading-edge shedding occurs.

For the incidence greater than 8°, smooth and turbulent flows produce the same results, due to the leading-edge vortex shedding.

Then, these measurements confirm that the reattachment on the lateral sides is strongly influenced by free-stream turbulence and the galloping properties should also be influenced. However, we do not have any measurements for intensities between 0.5% and 4.0%, although the Strouhal number shows a large modification. We do not really know whether this change is sudden or progressive. However, it may be expected that the flow regime, i.e. the morphology of the vortex shedding is modified abruptly by turbulence.

3.2. *Vibrations in low turbulence flow*

The vibration results in smooth flow are presented in Figs. 10–12 for the angles of attack 0, 2 and 4°, respectively. For 6° and above, the system remains stable to galloping which is explained by the change in the lift slope, as predicted with the so-called Den Hartog criterion [1].

The different symbols are related to different acquisition parameters in order to check the reproductibility. An important point of these measurements is the elimination of the hysteresis effect for each test. Each point presented in figures was performed starting with the beam held static; acquisition was then triggered after the stationary vibrations were reached.

The results show a resonant excitation with a third bending mode of the beam by vortex shedding at a reduced velocity $V_r = 60$. Classical resonance with the first

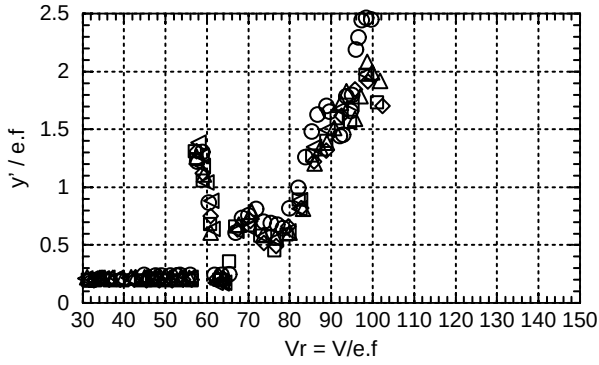

Fig. 10. Vibrations results at $\alpha = 0^\circ$ and $I = 0.5\%$.

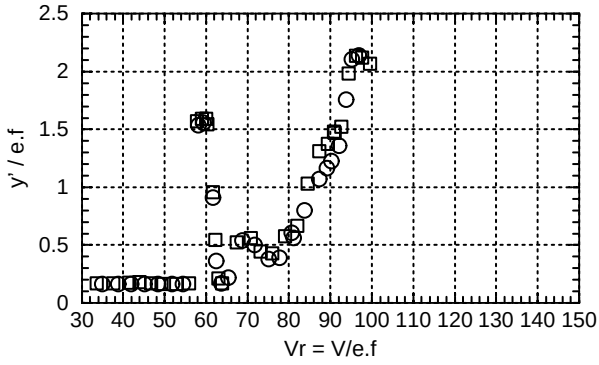

Fig. 11. Vibrations results at $\alpha = 2^\circ$ and $I = 0.5\%$.

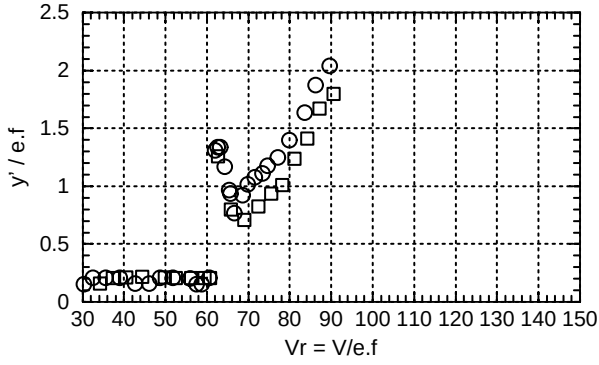

Fig. 12. Vibrations results at $\alpha = 4^\circ$ and $I = 0.5\%$.

mode could not be reached in this study because the corresponding wind velocity was too low to be performed by the tunnel facility. More details on this particular phenomenon can be found in Ref. [14]. It will disappear with the turbulent

flows because at least resonance does not occur due to the change in Strouhal frequency.

As for galloping, we observe a critical reduced velocity at about 65–70 for the three incidences. The accuracy of the critical velocity is perturbed by the vortex-shedding excitation although hysteresis effect was eliminated as mentioned previously.

It can be reasonably suspected that the vortex shedding may trigger the galloping oscillations earlier. However, since the shedding frequency is different from the bending mode excited by galloping [14], this hypothesis loses in likelihood.

For the galloping oscillations, the amplitude grows rapidly with the reduced velocity and experiments were stopped before damaging the system. These oscillations are based on the first bending mode as it can be observed in Figs. 13 and 14. These results are for $\alpha = 0^\circ$ and $V_r = 106$. The velocity in the wake shows a large peak on the frequency of the first mode. It is obvious that the vortex shedding is triggered by the galloping oscillations.

By comparison with the alternate vortex-induced oscillations at $V_r = 60$ [14], we note that the galloping regime produces only the peak on fundamental frequency in

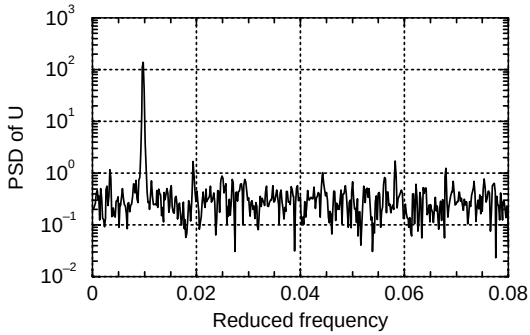

Fig. 13. Power spectral density of the longitudinal velocity in the wake of the vibrating cylinder.

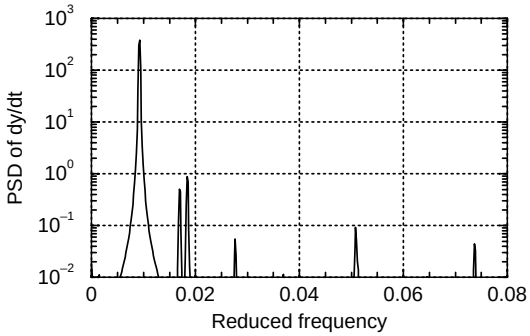

Fig. 14. Power spectral density of the cylinder velocity (the sensor is placed on mid-span of the cylinder).

the wake, whereas the vortex excitation produced in addition a number of harmonics.

Because only the first mode is involved in the movement, it is possible to deduce easily the corresponding displacement of the middle of the beam. As for example, a reduced vibration velocity of 2 (RMS) is equivalent to a reduced displacement of $2/2\pi$ (RMS). This value represents a maximum amplitude of ± 0.45 the thickness e of the beam.

3.3. Results in turbulent flow

The results of vibrations in turbulent flows are given Figs. 15–17 for the angles of attack 0, 2 and 4°. The system is always stable at 4° for the range of velocity performed, up to $V_r = 150$. The vortex-shedding excitation is not visible and Strouhal number measurements (Fig. 9) are helpful to admit that this kind of excitation does not occur.

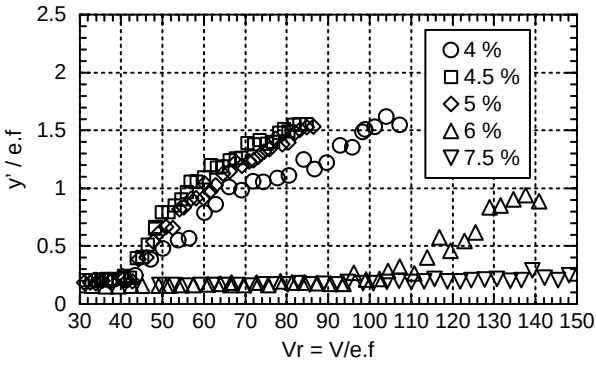

Fig. 15. Vibrations results at $\alpha = 0°$ in turbulent flows.

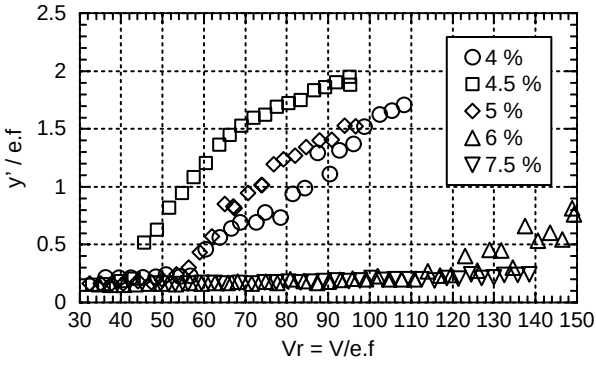

Fig. 16. Vibrations results at $\alpha = 2°$ in turbulent flows.

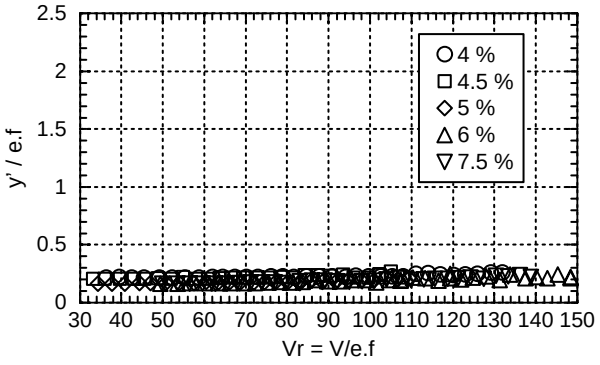

Fig. 17. Vibrations results at $\alpha = 4^\circ$ in turbulent flows.

For 7.5% of turbulence intensity, neither galloping oscillation was observed. This behaviour is consistent with the fact that the lift slope becomes positive for this range of turbulence, as shown by the results of Novak reported in Ref. [15].

At 0°, we observe a significant decrease of the critical velocity for the intensities 4–5% by comparison with smooth flow. Indeed, the value of V_r changes from 65 to 42 which represents a decrease of 35%. The uncertainty of the critical velocities in smooth flow, due to the vortex shedding excitation, is smaller than the gap reported here. It is really due to the change in turbulence intensity.

At 6%, the vibrations occur above $V_r = 110$ which is induced by the beginning of the reattachment of the flow on the lateral sides. The aerodynamic damping is less negative and the stability region is larger.

At 2° of incidence, the behaviour is almost the same as for 0°, with a shift of about $+10$ of the reduced critical velocity: the slope of the lift becomes less negative and so the aerodynamic damping decreases.

A strange result is the fact that the critical velocity at 4.5% of turbulence intensity remains the same as for 0°. This result can be perfectly reproduced and we may suspect an effect of a local stall due to the geometry of the corners of the section which are not rigorously sharp angles. However, this point is not clear completely.

For the incidence 4°, the system was found stable for every large intensity and velocity tested. The free-stream turbulence produces an earlier reattachment of the flow on the lateral sides which induces a positive slope of the lift curve.

Anyway, we have said that the present study was focused on the effects of the turbulence intensity. However, we can see in Fig. 6 that the longitudinal scale Lx is not constant versus the velocity, although it does not change from one level of intensity to another.

In the experiments of Ref. [2] on flat plates with rectangular leading edge, we can note that the reattachment of the flow occurs earlier when the scale is small. Increasing the scale moves back the reattachment point, which should generate an earlier galloping instability. The big change occurs for the value $Lx/e = 5$, which is inside our range of variation. Likewise, it was shown in Ref. [7], for rectangular

Table 1
Critical reduced velocities

Intensity (%)	$\alpha = 0^\circ$	$\alpha = 2^\circ$	$\alpha = 4^\circ$	$\alpha = 6^\circ$
$I = 0.5$	65	65	65	stable
$I = 4$	42	55	stable	stable
$I = 4.5$	42	42 (?)	stable	stable
$I = 5$	42	55	stable	stable
$I = 6$	110	120–130	stable	stable
$I = 7.5$	stable	stable	stable	stable

sections of large shape ratio ($c/e = 6.66$) that a critical value exists for Lx/e between 2.8 and 7.8.

In the present study, the critical value $Lx/e = 5$ corresponds to a reduced velocity between 81 and 96 (11–13 m/s in Fig. 6) for the turbulent flows. On the contrary, in smooth flow, the testing conditions are all over the critical scale value. Then the decrease of the critical velocity of the galloping instability, from smooth flow (0.5%) to the low turbulent flow (4%), as resumed in Table 1, cannot be attributed to an effect of the longitudinal scale. For higher intensity, between 5% and 6%, the critical velocity strongly increases and crosses the corresponding region, where the longitudinal scale may have an influence.

4. Conclusions

The main results of the study are the critical reduced velocities as reported in Table 1. At 0° and 2° of incidence, it appears that increasing the turbulence intensity (until 5%) first decreases the critical velocity from 65 down to 42. As we know, this phenomenon has not been reported before.

Then, when we further increase the intensity, the galloping occurs later and disappears for 7.5%, which is a classical result.

By comparison with measurements of previous authors, the longitudinal scale effect is not considered significant in our results: indeed, the variation which was performed on this parameter is small by comparison with the intensity and cannot really lead to some conclusions.

A modelling of galloping forces as suggested in Ref. [11] seems to be able to reproduce this phenomenon and will be investigated in detail in the future. The jump of the Strouhal number without and with turbulence is a useful and important information.

For the incidence 4°, the turbulence makes the system stable. It can be explained by the reattachment on the lateral sides which induces a flow similar to the one around sections of larger shape ratio.

However, all these conclusions should be taken keeping in mind the relative low Reynolds number of these experiments.

This study is completed by other specific investigations including:

- Experiments on the Vortex-Induced Vibrations in smooth flow, with hot wire measurements in the wake during lock-in [14].
- Numerical simulations are also performed for the non-moving structure and in both cases of vortex lock-in and galloping [16].

Acknowledgements

The Conservatoire National des Arts et Métiers (CNAM) is gratefully acknowledged for its support concerning the visit of professor Wojciechowski at the Institut Aérotechnique (IAT).

References

[1] J.P. Den Hartog, Mechanical Vibrations, 1985 Edition, Dover, New York, 1934, pp. 299–305.
[2] Q.S. Li, W.H. Melbourne, An experimental investigation of the effects of free-stream turbulence on streamwise surface pressures in separated and reattaching flow, J. Wind Eng. Ind. Aerodyn. 54/55 (1995) 313–323.
[3] Y. Nakamura, Y. Ohya, The effects of turbulence on the mean flow past square rods, J. Fluids Mech. 137 (1983) 331–345.
[4] Y. Nakamura, Y. Ohya, The effects of turbulence on the mean flow past two-dimensional rectangular cylinders, J. Fluids Mech. 149 (1984) 255–273.
[5] P. Saathoff, W.H. Melbourne, Effects of freestream turbulence on streamwise pressure measured on a square-section cylinder, J. Wind Eng. Ind. Aerodyn. 79 (1999) 61–78.
[6] I.S. Gartshore, The effects of free stream turbulence on the drag of rectangular two-dimensional prisms. BLWTL Report 4–73. University of Western Ontario, 1973.
[7] F.L. Haan, A. Kareem, A.A. Szewczyk, The effects of turbulence on the pressure distribution around a rectrangular prism, J. Wind Eng. Ind. Aerodyn. 77/78 (1998) 381–392.
[8] S. Deniz, T. Staubli, Oscillating rectangular and octogonal profiles: interaction of leading and trailing edge vortex formation, J. Fluids Struct. 11 (1997) 3–31.
[9] S. Deniz, T. Staubli, Oscillating rectangular and octogonal profiles: modelling of fluid forces, J. Fluids Struct. 12 (1998) 859–882.
[10] M. Matsumoto, et al., Aerodynamic effects of the angle of attack on a rectangular prism, J. Wind Eng. Ind. Aerodyn. 77/78 (1998) 531–542.
[11] P. Hémon, Approach of galloping vibrations using a time delayed force modelling and experimental validation, C. R. Acad. Sci. Paris Ser. II b 327 (1999) 679–684.
[12] J.O. Hinze, Turbulence, 2nd Edition, McGraw Hill, New York, 1975.
[13] C. Norberg, Flow around rectangular cylinders: pressure forces and wake frequencies, J. Wind Eng. Ind. Aerodyn. 49 (1993) 187–196.
[14] P. Hémon, F. Santi, Vortex induced vibrations of an elongated rectangular beam, in: S. Ziada, T. Staubli (Eds.), Flow-Induced Vibrations, Balkema, Rotterdam, 2000, pp. 123–130.
[15] E. Naudascher, D. Rockwell, Flow-Induced Vibrations an Engineering Guide, Balkema, Rotterdam, 1994, pp. 200–208.
[16] F. Santi, P. Hémon, Numerical investigation of flow-induced vibrations of an elongated rectangular cylinder in cross-flow. Presented at BBAAIV, Bochum, Germany, 11–14 September 2000.